Dalton Transactions

PAPER

View Article Online
View Journal | View Issue

Cite this: *Dalton Trans.*, 2016, **45**, 7443

Synthesis of mesoporous-silica-coated Gd_2O_3:Eu@silica particles as cell imaging and drug delivery agents†

Weiye Song, Weihua Di* and Weiping Qin*

Received 16th December 2015,
Accepted 21st March 2016

DOI: 10.1039/c5dt04908c

www.rsc.org/dalton

Mesoporous-silica-coated Gd_2O_3:Eu/silica nanoparticles were synthesized by a multistep chemical process and characterized by XRD, TEM and N_2 adsorption/desorption isotherms in terms of size, morphology and porosity. The core Gd_2O_3:Eu obtained by this method was highly luminescent upon excitation, giving the function of cell imaging upon incubation with the human cervical carcinoma (HeLa) cells. The outer porous silica shell is able to load the anticancer drug with a relatively high loading efficiency and release the loaded drugs at a sustained rate. The HeLa cells can be killed effectively on incubation with the core–shell porous particles loaded with the anticancer drug DOX. Meanwhile, the accumulation of mesoporous nanoparticles loaded with drugs in the target location could be monitored *via* fluorescence imaging. Therefore, the core–shell hybrid nanoparticles presented in this work are potential multifunctional biomaterials for smart detection or diagnosis and therapy in future biomedical engineering.

1. Introduction

Drug delivery systems offer numerous advantages compared with conventional formulations, such as improved efficacy, reduced toxicity, reduced frequency of doses, and ease of usage.[1–7] Of the different drug delivery systems reported, drug-loaded nanoparticles with mesoporous structures have attracted great attention because of their specific characteristics such as high surface area, tunable pore size and volume, well-defined surface properties and their injectable features.[8–13]

Despite many advantages of the mesoporous nanoparticles as an efficient drug delivery system, visualizing the accumulation of mesoporous nanoparticles loaded with drugs in target tissues is also equally critical for effective disease treatments. Recently, there has been an increased interest in the encapsulation of magnetic resonance imaging (MRI) contrast agents or fluorescent contrast agents into mesoporous carriers to provide dual capability of simultaneous imaging and drug delivery.[14–17]

MRI and/or optical imaging not only offers the ability to follow the distribution of nanocomposites containing drug carriers *in vitro*/*in vivo*, but also provides real-time monitoring on the drug delivery.[18–21] The formation of multifunctional composite structured materials is conventionally followed by an encapsulation process, where the magnetic/optical core is encapsulated or attached by/at the mesoporous shell.[22–29] The luminescent components are generally organic dyes or CdSe quantum dots (QDs). The photobleaching and quenching of dye molecules and the toxicity of QDs have seriously limited their applications in biomedical areas, especially for use in *in vivo*.[30–33]

As suitable alternatives for dyes and QDs, lanthanide-doped inorganic nanoparticles seem to be a promising fluorescent material for biodetection due to their good luminescence properties, high chemical and photochemical stability and low toxicity.[34–41]

In this work, we have designed and synthesized multifunctional hybrid materials with a lanthanide-based luminescent nanoparticle as the core and mesoporous silica as the shell by a multistep chemical process. The resulting particles are highly luminescent with an absolute emission quantum yield of 0.56. Upon cellular uptake, the particles display bright intracellular luminescence *via* incubation. The mesoporous shell is able to load and release the drug with a relatively high loading efficiency and a sustained release behavior. These features endow the particles with the dual functions of cell imaging and drug delivery.

State Key Laboratory on Integrated Optoelectronics, College of Electronic Science and Engineering, Jilin University, Changchun 130012, PR China.
E-mail: whdi@jlu.edu.cn, wpqin@jlu.edu.cn

†Electronic supplementary information (ESI) available: Characterization of the as-synthesized $Gd(OH)CO_3·H_2O$:Eu (FT-IR, TGA and elemental analysis); XRD pattern of the product obtained for $Gd(OH)CO_3·H_2O$:Eu upon calcination at 750 °C; the morphology of the HeLa cells incubated with the DOX-loaded mesoporous particles as a function of incubation time. See DOI: 10.1039/c5dt04908c

2. Experimental section

2.1. Preparation of $Gd(OH)CO_3{\cdot}H_2O$:Eu

The monodisperse $Gd(OH)CO_3{\cdot}H_2O$:Eu colloidal nanoparticles were prepared *via* a urea-based homogeneous precipitation process. A total of 5 mL of $Gd/Eu(NO_3)_3$ (1 M, Gd : Eu = 95 : 5) and 10 g of urea $[CO(NH_2)_2]$ were dissolved in deionized water. The total volume of the solution was about 250 mL. The above solution was first homogenized under magnetic stirring at room temperature for 2 h, and then reacted at 85 °C for 2.5 h in an oil bath. The obtained suspension was separated by centrifugation and collected after washing with deionized water and ethanol several times.

2.2. Preparation of core–shell $Gd(OH)CO_3{\cdot}H_2O$:Eu@SiO_2 particles

The core–shell $Gd(OH)CO_3{\cdot}H_2O$:Eu@SiO_2 particles were prepared *via* a modified Stöber sol–gel process. In a typical procedure, 50 mg of $Gd(OH)CO_3{\cdot}H_2O$:Eu particles were well dispersed in a mixture of 70 mL of ethanol and 20 mL of deionized water by ultrasonication for 30 min. 50 μL of tetraethoxysilane (TEOS) dispersed in 10 mL ethanol was added dropwise, followed by 1.0 mL of concentrated ammonia aqueous solution (28 wt%) to initiate the polycondensation process. The solution was continuously stirred at room temperature for 24 h. The obtained particles were separated and washed with ethanol and water, and then dried in a vacuum at room temperature.

2.3. Preparation of mesoporous-silica-coated Gd_2O_3@silica particles

40 mg of $Gd(OH)CO_3{\cdot}H_2O$:Eu@SiO_2 particles were well dispersed in a mixture of 50 mL of ethanol and 15 mL of deionized water by ultrasonication for 30 min. 100 μL of TEOS and 40 μL of octadecyltrimethoxysilane (C18TMS) were mixed and dispersed in the ethanol (10 mL) and ammonia hydroxide solution, and then added to the $Gd(OH)CO_3{\cdot}H_2O$:Eu@SiO_2 particles drop by drop and reacted by magnetic stirring for 12 h at room temperature. The particles were collected by centrifugation, washed with ethanol and water 3 times, and then dried at 50 °C overnight. The obtained particles were calcined at 650 °C for 6 h.

2.4. DOX loading

50 mg of mesoporous nanoparticles were mixed with 5 mL of DOX solution in phosphate-buffered saline (PBS, 0.4 mg mL^{-1}). After stirring for 24 h under dark conditions, the DOX-loaded particles were centrifuged and washed with PBS (5 mL) to remove the unloaded DOX. The particles were redispersed in PBS (1 mL) for subsequent tests of *in vitro* DOX release and cytotoxicity against HeLa cells. To evaluate the DOX-loading efficiency, UV–vis absorption spectroscopy was used to measure the absorption of the supernatant and the washed solutions at a wavelength of 233 nm.

2.5. DOX release

The above-prepared DOX-loaded particles (15 mg) were immersed in PBS (5 mL, pH 7.4 and 5.0) at 37 °C and shaken at 100 rpm. At certain time intervals, aliquots of PBS (5 mL) were taken out by centrifugation to test the concentration of released DOX and fresh PBS (5 mL) was added to the tube containing the DOX-loaded particles.

2.6. Cell culture

HeLa cell lines were maintained in Dulbecco's modified Eagle's medium (DMEM) containing 10% fetal bovine serum (FBS), penicillin (100 units per mL), and streptomycin (100 mg mL^{-1}). Cells were cultured with the complete medium in 5% CO_2 at 37 °C. For all experiments, cells were harvested from subconfluent cultures by the use of trypsin and were resuspended in fresh complete medium before plating.

2.7. Cellular uptake and observation

In a typical procedure, 7.5×10^4 cells were plated in a 35 mm Petri dish for 4 h to allow the cells to attach. After the cells were washed twice with PBS, mesoporous core–shell nanoparticles were added to the Petri dishes. After incubation for 4–24 h, the cells were washed several times with PBS to remove the remaining particles and dead cells, and then observed under a confocal fluorescence microscope (TCS SP5, Leica). For the observation of DOX-loaded nanoparticles incubated with HeLa cells, the same procedures were used.

2.8. Cytotoxicity assay

In vitro cytotoxicities were evaluated by performing 3-(4,5-dimethylthiazol-2-yl)-2,5-diphenyltetrazolium bromide (MTT) reduction assays on the HeLa cells. In a typical procedure, cells were seeded into 96-well culture plates at 7.5×10^4 per well in DMEM with 10% FBS at 37 °C under 5% CO_2 for 24 h; then the cells were incubated with core–shell particles loaded with the anticancer drugs at 37 °C under 5% CO_2 for different times. Thereafter, the medium containing the particles was removed, and an MTT solution (200 mL, diluted in a culture medium to a final concentration of 1 mg mL^{-1}) was added, and then the mixture was incubated for another 4 h. The medium was then replaced with dimethyl sulfoxide (200 mL), and the absorbance was monitored with a microplate reader at a wavelength of 570 nm. The cytotoxicity was expressed as the percentage of cell viability compared to that of untreated control cells. For the cytotoxic evaluation of DOX-loaded particles, similar procedures were used.

2.9. Chemico-physical characterization

The X-ray powder diffraction (XRD) data were collected on an X'Pert MPD Philips diffractometer (CuKα X-radiation at 40 kV and 50 mA) in the 2θ range from 10° to 70° with a scanning step of 0.02°. The transmission electron microscopy (TEM) observations were carried out using a JEOL 2200FS microscope. Samples for TEM investigations were prepared by first dispersing the particles in ethanol under the assistance of

ultrasonication and then dropping 1 drop of the suspension on a copper TEM grid coated with a holey carbon film. Fourier transform infrared (FT-IR) spectra (Mattson 5000) of the samples were recorded in the range of 4000–500 cm^{-1} in transmission mode. The pellets were prepared by adding 0.8 mg of the sample powder to 80 mg of KBr. The powders were mixed homogeneously and compressed at a pressure of 10 kPa to form transparent pellets. Thermogravimetric analysis (TGA) of the as-prepared precursor was performed using a thermoanalyzer (Thermo Plus TG 8120, Rigaku). The data were recorded at a scan rate of 5 °C min^{-1} from room temperature to 800 °C in air. The N_2 adsorption–desorption isotherms were recorded at 77 K on a Micromeritics ASAP 2010. The samples were degassed at 523 K and 10^{-6} torr for 10 h prior to measurement. UV–vis absorbance measurements were carried out by using a single-beam spectrophotometer (U-2900, Hitachi) equipped with a 75 W pulsed xenon lamp with a scan rate of 240 nm min^{-1}. The fluorescence spectra were recorded on a fluorescence spectrophotometer (F-7000, Hitachi) at room temperature. The slit widths of the excitation and emission were both 1.0 nm. The luminescence quantum yield was measured on a Fluorescence SENS-9000 PL calibrated spectrometer equipped with an integrated sphere. Three measurements were made for each sample and the average value is reported. The method is accurate to within 5%.

3. Results and discussion

3.1. $Gd(OH)CO_3·H_2O$:Eu as precursor

Eu^{3+}-doped gadolinium hydroxylcarbonate ($Gd(OH)CO_3·H_2O$:Eu) was prepared *via* a urea-based homogeneous precipitation method (Experimental section), in which urea serves as a precipitation agent of metal cations due to self-decomposition into OH^- and CO_3^{2-} at elevated temperatures (>83 °C). Urea-based precipitation is a simple and general route for the preparation of lanthanide hydroxylcarbonate that was first developed by Matijevic and coworkers.[42] Fourier transform infrared spectroscopy (FTIR, Fig. S1, ESI†), thermogravimetric analysis (Fig. S2, ESI†) and elemental analysis (Table S1, ESI†) confirmed that the chemical composition of the as-prepared precursor is $Gd(OH)CO_3·H_2O$:Eu. X-ray diffraction (XRD) measurement revealed that the as-prepared precursor material is amorphous (not shown). These results are consistent with the pioneering work of Matijevic *et al.*[42] The transmission electron microscopy (TEM) observation (Fig. 1(a)) revealed that the as-prepared $Gd(OH)CO_3·H_2O$:Eu particles appear spherical and nearly monodispersed. The size distribution plot (Fig. 1(b)) based on the analysis of 100 particles from TEM observations indicates that the spherical particle size ranges from 130 to 170 nm with an average diameter of 150 nm and a standard deviation of ±10.6%. The spherical particles with homogeneous monodispersed distribution are preferred for further surface modifications as they facilitate uniform surface conjugation.[43]

3.2. Mesoporous-SiO_2-coated Gd_2O_3:Eu@SiO_2 particles

Mesoporous-silica-coated Gd_2O_3:Eu@SiO_2 nanoparticles were synthesized by a multistep process: (1) the coating of the first layer of silica onto the $Gd(OH)CO_3·H_2O$:Eu particles to form $Gd(OH)CO_3·H_2O$:Eu@SiO_2 core–shell particles; (2) another layer of silica coating onto the $Gd(OH)CO_3·H_2O$:Eu@SiO_2 particles *via* a modified Stöber process in the presence of TEOS and C18TMS; (3) subsequent thermal decomposition *via* calcination that results in the conversion of $Gd(OH)CO_3·H_2O$:Eu to Gd_2O_3:Eu and the formation of mesoporous silica.

The core–shell structure of the particles after coating can be clearly seen by TEM due to the different electron contrast for the cores and shells (Fig. 2(a) and (b)). The inner dark and outer gray regions correspond to the Gd_2O_3 core and SiO_2 shell, respectively. It can be seen that the first layer of silica was grown around each Gd_2O_3 particle and no separated SiO_2 particles were formed. The first SiO_2 shell was homogeneous and the thickness is about 20 nm, as marked in Fig. 2(b). The easy and homogeneous growth of the first silica shell can be attributed to the composition of the core $Gd(OH)CO_3·H_2O$. As a matter of fact, due to the hydrated phase and the presence of hydroxyl groups, TEOS can easily react with the surface of the core particles forming a first silica monolayer on top of which the silica shell can easily grow *via* the Stöber process.

Mesoporous silica were coated onto the $Gd(OH)CO_3·H_2O$@SiO_2 core–shell structured nanoparticles *via* a

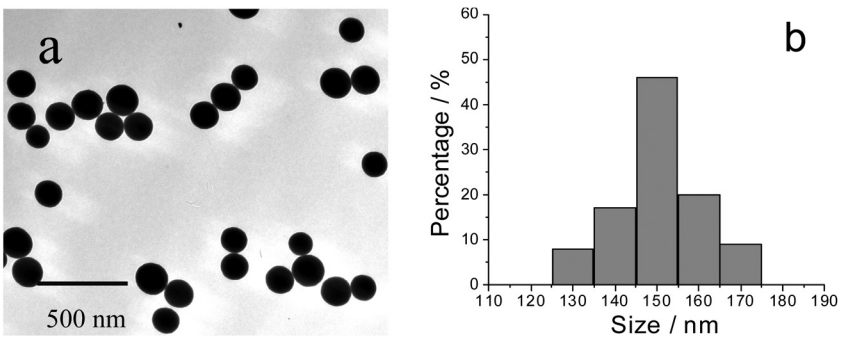

Fig. 1 TEM images of the spherical $Gd(OH)CO_3·H_2O$:Eu particles (a) and the size distribution plot based on the analysis of 100 particles from TEM observations (b).

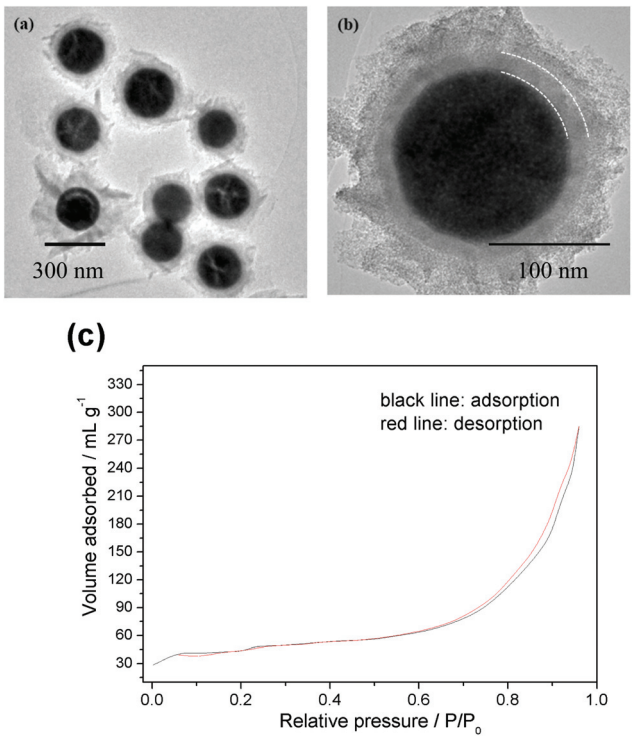

Fig. 2 TEM images (a and b) and nitrogen adsorption–desorption isotherm (c) of mesoporous-SiO_2-coated Gd_2O_3:Eu@SiO_2.

modified well known protocol through the cocondensation of TEOS and C18TMS followed by calcination at 650 °C,[44] as revealed by TEM (Fig. 2(b)). The double-shell structure can also be clearly observed. The mesoporous nature of the sample was further revealed by the N_2 adsorption–desorption isotherm, as shown in Fig. 2(c). The isotherm could be classified as a type-IV isotherm according to the International Union of Pure and Applied Chemistry (IUPAC) nomenclature.[16,45] Simultaneously, the core $Gd(OH)CO_3{\cdot}H_2O$ was converted and crystallized into gadolinium oxides from the amorphous $Gd(OH)CO_3{\cdot}H_2O$:Eu upon calcination at 650 °C (see XRD, Fig. S3, ESI†). Thus, mesoporous-SiO_2-coated Gd_2O_3:Eu@SiO_2 particles were formed *via* such a multistep reaction process.

3.3. Luminescence

The luminescence of mesoporous-silica-coated Gd_2O_3:Eu@SiO_2 particles was measured and is shown in Fig. 3. In the excitation spectrum (red line), a broad band centered at 255 nm originates from the excitation of the oxygen-to-europium charge transfer band (CTB). The presence of the Gd^{3+} $^8S_{7/2} \rightarrow {}^6I_j$ transition located at ~277 nm suggests the existence of Gd^{3+}-to-Eu^{3+} energy transfer.[46] The weak peaks in the longer wavelength 280–570 nm region are ascribed to the direct f–f transitions within the Eu^{3+} $4f^6$ electron configuration. Upon excitation into a maximum of CTB, the characteristic transition lines could be detected in the emission spectra ranging from 575 to 725 nm due to the Eu^{3+} $^5D_0 \rightarrow {}^7F_j$ (j = 0,1,2,3,4) transitions. The photoluminescence features were

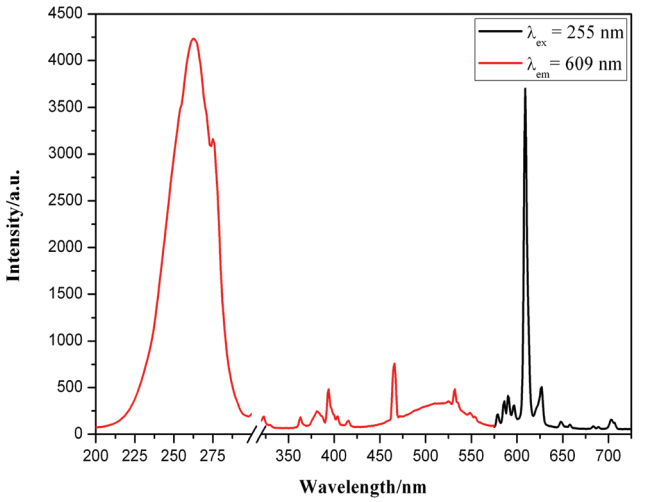

Fig. 3 Photoluminescence excitation and emission spectra of mesoporous Gd_2O_3:Eu (5 mol% doping) at room temperature.

further quantified through the estimation of the absolute emission quantum yield that was measured on a calibrated spectrometer equipped with an integrated sphere. The quantum yield acquired was as high as ~0.56 upon excitation at 255 nm. Such high quantum yield obtained for the mesoporous-SiO_2-coated Gd_2O_3:Eu@SiO_2 was attributed to the conversion of amorphous $Gd(OH)CO_3{\cdot}H_2O$:Eu to the crystalline Gd_2O_3:Eu and the removal of H_2O molecules and hydroxyl groups as luminescence quenchers by calcination.[47] A drop of the core–shell particles dispersed in ethanol was smeared on the surface of a glass slide for observation using a laser scanning confocal microscope. Fig. S4 (ESI†) shows a luminescence photograph of the core–shell particles upon optical excitation. The particles are clearly visible due to bright red emission from the core Gd_2O_3:Eu. Strong luminescence particularly benefits the biological use as fluorescent labels.

The possibility of the use of mesoporous-SiO_2-coated Gd_2O_3:Eu@SiO_2 particles as luminescent biological labels was checked by *in vitro* biological experiments using human cervical carcinoma (HeLa) cells. A two-photon laser scanning confocal microscope operating at around a 380 nm excitation wavelength was applied to excite the Eu^{3+} dopants for luminescence. Upon incubation, the uptake of mesoporous-SiO_2-coated Gd_2O_3:Eu@SiO_2 particles by HeLa cells was observed. Fig. 4 shows bright-field optical and fluorescence microscopy images of HeLa cells after incubation with 0.2 mg mL^{-1} of particles for 24 h. As observed, the particles can be taken up by the HeLa cells and display bright luminescence (Fig. 4b). This indicates that these mesoporous nanoparticles clearly retained their intrinsic fluorescence upon cellular uptake.

3.4. *In vitro* drug storage and release

Mesoporous silica particles are excellent drug carriers because of their noncytotoxic properties. In our *in vitro* experiments, we selected a typical and widely used anticancer drug, doxo-

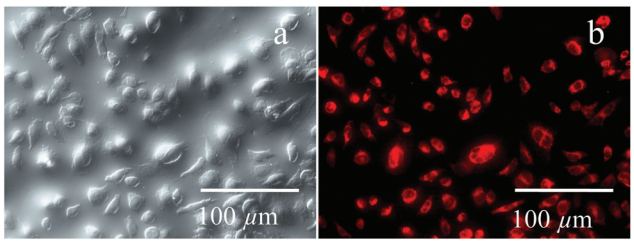

Fig. 4 Bright-field (a) and fluorescence microscopy (b) images of HeLa cells incubated with mesoporous-SiO_2-coated Gd_2O_3:Eu@SiO_2 particles for 24 h.

rubicin hydrochloride (DOX), to investigate drug storage and release behavior of the mesoporous-SiO_2-coated Gd_2O_3:Eu@SiO_2 particles. The mesoporous core–shell nanoparticles were loaded with DOX by soaking them in a concentrated drug–PBS (phosphate-buffered saline, pH 7.4) solution. The drug-loaded particles were collected by centrifugation and washing several times followed by drying under vacuum. The drug loading content was evaluated by comparing the UV-vis absorption of the supernatant and washed solutions with that of the original DOX solution at a wavelength of 233 nm. Based on absorption measurements, approximately 29.2 μg of drug molecules were stored inside 1 mg of mesoporous particles. The loading efficiency of DOX was calculated as follows: $E\% = (O_{DOX} - R_{DOX})/O_{DOX} \times 100\%$, where O_{DOX} and R_{DOX} are the original and residual DOX content, respectively. The loading efficiency of DOX was 73%, indicating a relatively high loading efficiency of our present mesoporous-silica-coated core–shell particles. To evaluate the release behavior of DOX-loaded particles, the particles were redispersed in PBS solution at 37 °C. Similarly, the drug release content was evaluated by using UV–vis absorption spectroscopy. Fig. 5 shows the drug release profile in the PBS with different pH values as a function of time. Initially, the drug loaded particles exhibit a fast delivery with ~52 wt% drug release within 8 h (pH 7.4 PBS); then the drug release ratio was ~32% during the subsequent 88 h, achieving a total release of ~84% of DOX within 96 h. By comparison, a relatively fast drug release in the pH 5.0 PBS was observed, which might be attributed to the decrease of interaction forces between DOX and the mesopore surface in the pH 5.0 PBS.[48] This indicates that our present mesoporous core–shell particles loaded with DOX obviously had a sustained drug release behavior, and such kinetics would be especially useful for effective treatment of serious diseases. These results demonstrate that the present mesoporous particles can be potentially used as an efficient vehicle to load and deliver anticancer drugs into cancer cells.

3.5. Pharmacological effect

To verify whether the released DOX was pharmacologically active, the cytotoxic effect of the DOX-loaded particles against HeLa cells was assessed using MTT reduction assays. Fig. 6 shows the cell viabilities against DOX-loaded particles. We can see that the DOX-loaded particles induced a significant cytotoxicity while incubated with the HeLa cells, which was demonstrated by the decreased cell viability upon incubation. The mesoporous-silica-coated Gd_2O_3:Eu@silica particles alone are almost nontoxic (Fig. S5, ESI†). This indicates that the cytotoxic effect originates from the release of drug molecules inside the cancer cells.

In detail, the viabilities of HeLa cells depend on the concentration of DOX loaded into the mesoporous particles. A higher concentration of DOX leads to the death of more HeLa cells. On the other hand, the viabilities of HeLa cells are also dependent on the incubation time. Taking the mesoporous particles loaded with 20 μg DOX, a short-time (6 h) exposure led to an ~20% decrease in cell viability. Nearly 50% cells were

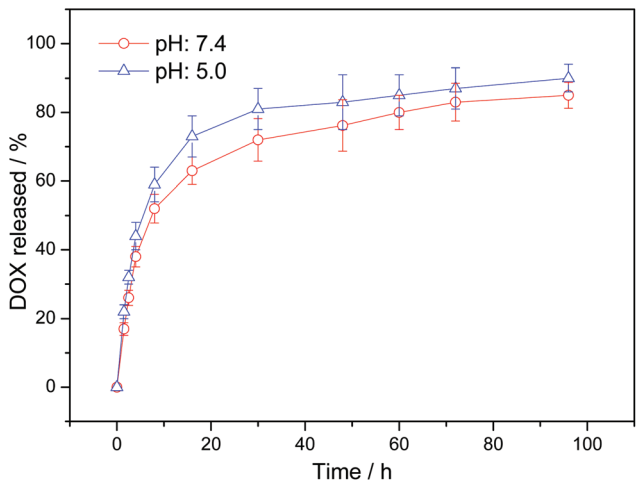

Fig. 5 Release profile of DOX from DOX-loaded mesoporous-SiO_2-coated Gd_2O_3:Eu@SiO_2 particles in PBS at 37 °C.

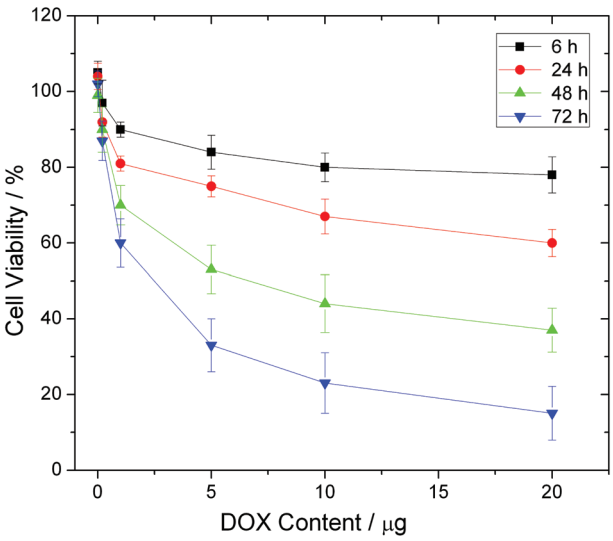

Fig. 6 The viability of HeLa cells incubated with DOX-loaded mesoporous-silica-coated Gd_2O_3:Eu@silica as a function of DOX concentration and incubation time.

alive after 48 h and the death rate of cells reached above 85% after 72 h incubation (Fig. 6).

Consistently, the morphology study of HeLa cells incubated with DOX-loaded mesoporous particles was performed using a bright field optical microscope (Fig. S6, ESI†). The cells before interaction with DOX-loaded particles were viable, well attached onto the plate and showed a clear profile. However, upon incubation with DOX-loaded particles, the HeLa cells shrank gradually and their profiles became vague, and were finally prone to death with an increase of incubation time. The number of viable cells observed decreases markedly with the increase of incubation time.

4. Conclusions

Mesoporous-silica-coated Gd_2O_3:Eu@silica particles were synthesized by a multistep chemical process. First, spherical and monodispersed $Gd(OH)CO_3{\cdot}H_2O$:Eu particles were prepared *via* a urea-based homogeneous precipitation method, and then two layers of silica were coated onto the surface of $Gd(OH)CO_3{\cdot}H_2O$ particles to form core–shell structures *via* a modified Stöber process. Finally, thermal decomposition of core–shell samples *via* a calcination process results in the conversion of $Gd(OH)CO_3{\cdot}H_2O$:Eu to Gd_2O_3:Eu and the formation of mesoporous silica. Thus, mesoporous-silica-coated Gd_2O_3@silica nanoparticles were formed. The present mesoporous core–shell nanoparticles have the capabilities of loading and releasing the drug with a relatively high loading efficiency and a sustained release behavior of drugs. The DOX-loaded porous core–shell particles are able to kill the cancer cells efficiently upon incubation with the human cervical carcinoma cells, indicating the potential for treatment of cancer cells. Meanwhile, these core–shell particles are intrinsically luminescent due to f–f transition of lanthanide ions upon excitation. They can be taken up by the cancer cells and emit the light *via* incubation with the HeLa cells. This indicates that the mesoporous-silica-coated Gd_2O_3:Eu@silica nanoparticles can be used as cell imaging agents and the drug delivery behavior can also be effectively monitored *via* luminescence imaging, thus achieving the multifunctionality of drug delivery and simultaneous imaging that were combined into a single nanoparticle.

Acknowledgements

This work was supported by the National Natural Science Foundation of China (grant no. 61178073).

References

1 Y. Wang, V. Bansal, A. Zelikin and F. Caruso, *Nano Lett.*, 2008, **8**, 1741.
2 W. Meier, *Chem. Soc. Rev.*, 2000, **29**, 295.
3 F. Caruso, R. Caruso and H. Mohwald, *Science*, 1998, **282**, 1111.
4 T. Zhang, J. Ge, Y. Hu, Q. Zhang, S. Aloni and Y. Yin, *Angew. Chem., Int. Ed.*, 2008, **47**, 5806.
5 C. L. Tao, Y. F. Zhu, Y. Xu, M. Zhu, H. Morita and N. Hanagata, *Dalton Trans.*, 2014, **43**, 5142.
6 R. Whitmire, D. Wilson, A. Singh, M. Levenston, N. Murthy and A. Garcia, *Biomaterials*, 2012, **33**, 7665.
7 Y. Zhu, J. Shi, W. Shen, X. Dong, J. Feng, M. Ruan and Y. Li, *Angew. Chem., Int. Ed.*, 2005, **44**, 5083.
8 C. Kresge, M. Leonowicz, W. Rhth, J. Vartuli and J. Beck, *Nature*, 1992, **359**, 710.
9 V. Torchilin, *Pharm. Res.*, 2007, **24**, 1.
10 M. Hartmann, *Chem. Mater.*, 2005, **17**, 4577–4593.
11 I. Candel, E. Aznar, L. Mondragon, C. de la Torre, R. Martinez-Manez, F. Sancenon, M. Marcos, P. Amoros, C. Guillem, E. Perez-Paya, A. Costero, S. Gil and M. Parra, *Nanoscale*, 2012, **4**, 7237.
12 X. M. Li, L. Zhou, Y. Wei, A. M. EI-Toni, F. Zhang and D. Y. Zhao, *J. Am. Chem. Soc.*, 2015, **137**, 5903.
13 M. Vallet-Regí, F. Balas and D. Arcos, Mesoporous Materials for Drug Delivery, *Angew. Chem. Int. Ed.*, 2007, **46**, 7548–7558.
14 M. Liong, J. Lu, M. Kovochich, T. Xia, S. Ruehm, A. Nel, F. Tamanoi and J. Zink, *ACS Nano*, 2008, **5**, 889.
15 Z. Jiang, B. Dong, B. Chen, J. Wang, L. Xu, S. Zhang and H. Song, *Small*, 2013, **9**, 604.
16 D. Yang, X. Kang, P. Ma, Y. Dai, Z. Hou, Z. Cheng, C. Li and J. Lin, *Biomaterials*, 2013, **34**, 1601.
17 X. M. Li, L. Zhou, Y. Wei, A. M. EI-Toni, F. Zhang and D. Y. Zhao, *J. Am. Chem. Soc.*, 2014, **136**, 15086.
18 P. Prabhu and V. Patravale, *J. Biomed. Nanotechnol.*, 2012, **8**, 859.
19 M. Janowski, J. Bulte and P. Walczak, *Adv. Drug Delivery Rev.*, 2012, **64**, 1488.
20 Y. Shao, X. Tian, W. Hu, Y. Zhang, H. Liu, H. He, Y. Shen, F. Xie and L. Li, *Biomaterials*, 2012, **33**, 6438.
21 J. Jung, M. Kim, J. Cho, S. Lee, I. Yang, J. Cho, S. Kim, C. Lee and J. Park, *Biomaterials*, 2012, **33**, 5865.
22 X. Qiao, J. Zhou, J. Xiao, Y. Wang, L. Sun and C. Yan, *Nanoscale*, 2012, **4**, 4611.
23 Y. F. Zhu, F. J. Shang, B. Li, Y. Dong, Y. F. Liu, M. R. Lohe, N. Hanagata and S. Kaskel, *J. Mater. Chem. B*, 2013, **1**, 1279.
24 S. Cheng, C. Lee, M. Chen, J. Souris, F. Tseng, C. Yang, C. Mou, C. Chen and L. Lo, *J. Mater. Chem.*, 2010, **20**, 6149.
25 I. Slowing, B. Trewyn, S. Giri and V. Lin, *Adv. Funct. Mater.*, 2007, **17**, 1225.
26 X. M. Li, F. Zhang and D. Y. Zhao, *Chem. Soc. Rev.*, 2015, **44**, 1346.
27 J. Fan, G. Fang, X. Wang, F. Zeng, Y. Xiang and S. Wu, *Nanotechnology*, 2011, **22**, 455102.
28 K. Wu, Y. Yang, Y. Liang, H. Chen, E. Sung, Y. Yamauchi and F. Lin, *Curr. Nanosci.*, 2011, **7**, 926.
29 J. Wang, Y. Lu, F. Peng, Y. Zhong, Y. Zhou, X. Jiang, Y. Su and Y. He, *Biomaterials*, 2013, **34**, 9509.

30 I. Gorelikov, A. Martin, M. Seo and N. Matsuura, *Langmuir*, 2011, **27**, 15024.
31 J. Pan, D. Wan and J. Gong, *Chem. Commun.*, 2011, **47**, 3442.
32 A. Celik, U. Comelekoglu and S. Yalin, *Toxicol. Ind. Health*, 2005, **21**, 243.
33 A. M. Derfus, W. C. W. Chan and S. N. Bhatia, *Nano Lett.*, 2004, **4**, 11.
34 S. Setua, D. Menon, A. Asok, S. Nair and M. Koyakutty, *Biomaterials*, 2010, **31**, 714.
35 S. Rodriguez-Liviano, A. Becerro, D. Alcántara, V. Grazú, J. de la Fuente and M. Ocaña, *Inorg. Chem.*, 2013, **52**, 647.
36 W. Di, J. Li, N. Shirahata, Y. Sakka, M. Willinger and N. Pinna, *Nanoscale*, 2011, **3**, 1263.
37 J. Shen, L. Sun, J. Zhu, L. Wei, H. Sun and C. Yan, *Adv. Funct. Mater.*, 2010, **20**, 3708.
38 Y. Wang, L. Ji, B. Zhang, P. Yin, Y. Qiu, D. Song, J. Zhou and Q. Li, *Nanotechnology*, 2013, **24**, 175101.
39 D. M. Yang, P. A. Ma, Z. Y. Hou, Z. Y. Cheng, C. X. Li and J. Lin, *Chem. Soc. Rev.*, 2015, **44**, 1416.
40 W. Zheng, P. Huang, D. T. Tu, E. Ma, H. M. Zhu and X. Y. Chen, *Chem. Soc. Rev.*, 2015, **44**, 1379.
41 P. Huang, W. Zheng, S. Y. Zhou, D. T. Tu, Z. Chen, H. M. Zhu, R. F. Li, E. Ma, M. D. Huang and X. Y. Chen, *Angew. Chem., Int. Ed.*, 2014, **53**, 1252.
42 E. Matijevic and W. Hsu, *J. Colloid Interface Sci.*, 1987, **118**, 506.
43 H. Cho, Z. Dong, G. Pauletti, J. Zhang, H. Xu, H. Gu, L. Wang, R. Ewing, C. Huth, F. Wang and D. Shi, *ACS Nano*, 2010, **4**, 5398.
44 H. Qian, H. Guo, P. Ho, R. Mahendran and Y. Zhang, *Small*, 2009, **5**, 2285.
45 K. Sing, D. Everett, R. Haul, L. Moscou, R. Pierotti, J. Rouquerol and T. Siemieniewska, *Pure Appl. Chem.*, 1985, **57**, 603.
46 S. Lv, J. Zhang, J. Zhang, H. Zhao, Y. Luo and X. Ren, *Nanotechnology*, 2010, **21**, 365709.
47 W. Di, X. Wang, B. Chen, S. Lu and X. Zhao, *J. Phys. Chem. B*, 2005, **109**, 13154.
48 Y. F. Zhu and C. L. Tao, *RSC Adv.*, 2015, **5**, 22365.